Biointerface Research in Applied Chemistry
Open-Access Journal (ISSN: 2069-5837)

Article
Volume 13, Issue 6, 2023, 545
https://doi.org/10.33263/BRIAC136.545

Thin Film Potential $Ba_{0.5}Sr_{0.5}TiO_3$ (BST) doped with RuO_2 6% as a Light Detecting Sensor at Solar Tracker ALSINTAN System in Microcontroller-Based

Ridwan Siskandar [1,*], Tineke Mandang [2,*], Wawan Hermawan [2], Irzaman Irzaman [3]

[1] Doctoral Student of Agricultural Engineering Science of Study Program, Department of Mechanical and Biosystem Engineering, Faculty of Agricultural Engineering and Technology, IPB University, Bogor, West Java 16680, Indonesia; ridwansiskandar@apps.ipb.ac.id; rsiskandar@apps.ipb.ac.id (R.S.);
[2] Department of Mechanical and Biosystem Engineering, Faculty of Agricultural Engineering and Technology, IPB University, Bogor, West Java 16680, Indonesia; tineke_mandang_2003@yahoo.com (T.M.); w_hermawan@apps.ipb.ac.id (W.H.);
[3] Department of Physics, Faculty of Mathematics and Science, IPB University, Meranti Street, Dramaga, Bogor, West Java 16680, Indonesia; irzaman@apps.ipb.ac.id (I.I.);
* Correspondence: ridwansiskandar@apps.ipb.ac.id (R.S.); tineke_mandang_2003@yahoo.com (T.M.);
Scopus Author ID 57188999030
Received: 6.08.2022; Accepted: 4.10.2022; Published: 8.02.2023

Abstract: In this article, we describe the potential application of 6% Rubium Dioxide (RuO_2) doped Barium Strontium Titanate (BST) thin film as an automatic integrated light detection sensor based on the ESP32 microcontroller. BST + RuO_2 6% thin films were made using the chemical solution deposition method followed by a spin coating which was then annealed at various temperatures (800°C, 850°C, and 900°C). We have confirmed that the BST + RuO_2 6% thin film with an annealing temperature of 850°C is the best thin film which is then applied to the solar tracker system for ALSINTAN. We assume that changes in the lattice parameters of its tetragonal crystal structure caused by variations in the annealing temperature result in different ion-transfer characteristics that induce charge polarization in the crystal structure. Thin film BST + RuO_2, 6% with an annealing temperature of 850oC, resulted in a low hysteresis curve with a hysteresis index of 0.02%. We assume the low hysteresis comes from the thin-film paraelectric phase at room temperature. Where in this phase, the thin film is observed at temperatures above the curie temperature. Another thing shows that 6% BST + RuO_2 thin film with an annealing temperature of 850°C also has a relatively more consistent output voltage value for two weeks of measurement. This shows that this thin film's strength/life span is good for application as a light detection sensor for ALSINTAN. In addition, it was found that 6% BST + RuO_2 thin film with an annealing temperature of 850°C had the highest detection range. Furthermore, we have clarified that the innovation casing design model is the best design model that is suitable to be applied to the solar tracker system for ALSINTAN. Then, we also found that based on the output voltage and current data generated from the measurement six times (at 08.00 AM; 09.00 AM; 10.00 AM; 11.00 AM; 12.00 AM; 01.00 PM; 02.00 PM; 03.00 PM, and 04.00 PM), the implementation of the solar tracker system is much better than without a solar tracker. The results of the power optimization calculation found that the use of a solar tracker and those without a solar tracker have a power difference of 37.21%.

Keywords: $Ba_{0.5}Sr_{0.5}TiO_3$ (BST); RuO_2 6%; annealing temperature; light detection sensor; solar tracker.

1. Introduction

Ferroelectric materials are one of the interesting advanced materials research topics because of their wide application in various fields. The main property of ferroelectric materials is that they are spontaneously polarized dielectrics and can change polarization due to certain external disturbances. For example, by utilizing a high dielectric constant, ferroelectric materials are applied as components for data storage, their piezoelectric properties are used as smart sensors and actuators, and their pyroelectric properties are applied in solar cells and smart temperature and light sensors [1–6].

A thin film is a layer of material with a thickness in the order of 10^{-9} m to 10^{-6} m, which is grown on a certain substrate. The material layer can be made of organic, inorganic, metal, or organic metal mixtures (organometallic) with conductor, semiconductor, superconducting, and insulating properties [7,8]. In its development, the material layer on a thin film is one of the objects of research because it can be used to produce a new generation of devices due to its unique characteristics/properties [2,9,10]. Barium Strontium Titanate (BST) is a ferroelectric ceramic material with various advantages, including a high dielectric constant, piezoelectric and pyroelectric characteristics, high electro-optic coefficient, environmentally friendly, and a chemically stable material [11].

BST is classified as an inorganic material that is ferroelectric. In its application, the BST layer can be grown on certain substrates using the following techniques: Chemical Solution Deposition (CSD) [12–14], Sputtering [15,16], Metal Organic Chemical Vapor Deposition (MOCVD) [17], Sol-Gel [18]. In this research, the fabrication of a thin layer of BST (with 6% RuO_2 byproduct) on a p-type Si(100) substrate using the Chemical Solution Deposition (CSD) technique and using a spin coater for the process of distributing the thin layer on the substrate surface as well as through variation of annealing process (800^{o}C, 850^{o}C, and 900^{o}C) [4,5,19,20].

The use of metal compounds as a binder is an effective way to modify the electrical and optical properties of BST [21]. One of the benefits of doping is reducing the energy gap's value, thereby increasing changes in the electric dipole moment and spontaneous polarization of the BTO thin film, which leads to the application of BTO as a smart sensor. Several doping uses have been reported, namely Chromium (Cr) [22], Terbium (Tb) [23], Lanthanum (La) [24], Tungsten (W) [25], and Cesium Oxide (CeO_2) compounds [20].

On the other hand, the use of renewable energy derived from solar energy is an interesting research topic to study, one of which is the optimization of solar panel-based electric battery charging [26] in his research explained that the movement of the sun's rotation in 1 day needs to be considered to get optimization of battery charging. This is in line with research [27], which explains that battery charging through solar panels is faster if it follows the movement of the sun's rotation. It is just that the weakness of this research is the sensitivity of the light sensor is not good, and the lifetime of the sensor can not be used continuously for reading the intensity of the sun.

Based on the above background, the hypothesis of this research is to add a binding element of RuO_2 to BST grown on p-type Si(100) substrate using the Chemical Solution Deposition (CSD) technique by utilizing a spin coater for the process of even distribution of the thin layer and variations annealing (800 ^{o}C, 850 ^{o}C, and 900 ^{o}C) to grow properties that can change the crystal structure of BST to produce thin films with light-sensitive spectra as light detecting sensors. This sensor is then used in the solar tracker system for Agricultural

Equipment/Machinery (ALSINTAN) as an optimization solution for ALSINTAN's battery charging.

2. Materials and Methods

2.1. BST thin film fabrication doped with RuO_2 6%.

This research was carried out in the electronic materials laboratory of the Department of Physics, FMIPA IPB University, and the hardware laboratory Computer Engineering Study Program, College of Vocational Studies, IPB University. The manufacture of thin films is divided into three stages: Calculation and preparation of $Ba_{0.5}Sr_{0.5}TiO_3$ solution materials with 6% RuO_2, Weighing and mixing of $Ba_{0.5}Sr_{0.5}TiO_3$ solution materials with 6% RuO_2, and growing $Ba_{0.5}Sr_{0.5}TiO_3$ thin films in 6% RuO_2 doped. More details on the process of making BST thin films in 6% RuO_2 are shown in Figure 1.

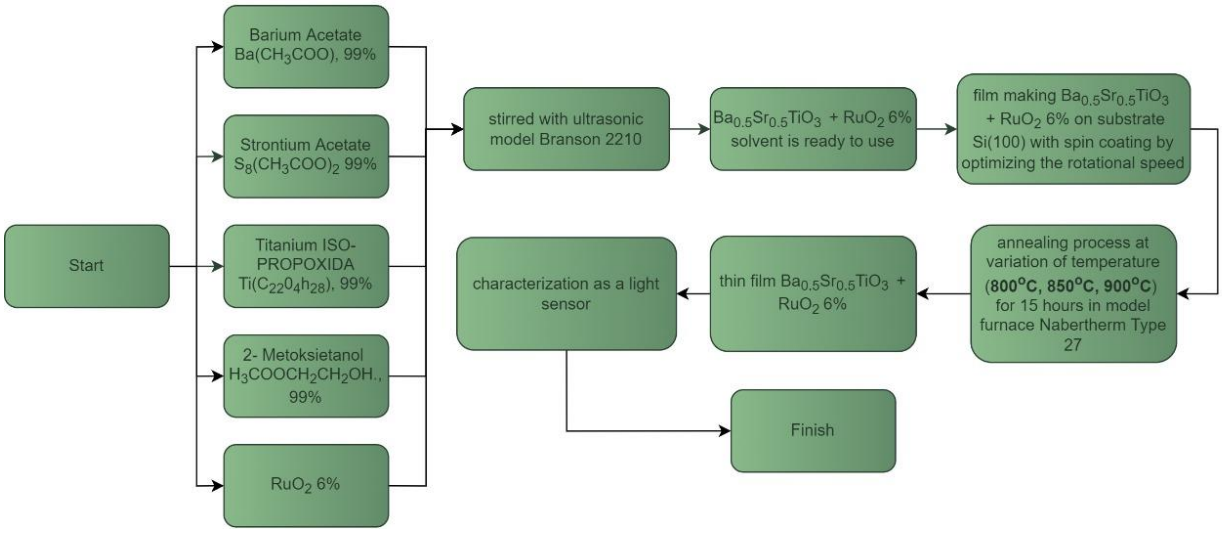

Figure 1. Flowchart BST hin film fabrication dotted with RuO_2 6%.

2.1.1. Calculation and preparation of solution materials $Ba_{0.5}Sr_{0.5}TiO_3$.

In this study, the thin film manufacturing process was divided into three stages. The first stage is the process of calculating and preparing the materials used to solve $Ba_{0.5}Sr_{0.5}TiO_3$. $Ba_{0.5}Sr_{0.5}TiO_3$ solution is obtained by mixing the chemicals according to the following balanced equation:

$$xBa(CH_3COO)_2 + (1\text{-}x)\ Sr(CH_3COO)_2 + Ti(OCH(CH_3)_2)_4 + y\ O_2 \rightarrow BaxSr1\text{-}xTiO_3 + z\ H_2O + v\ CO_2$$

Based on the results of balancing the reaction equation, to solve $Ba_{0.5}Sr_{0.5}TiO_3$ Barium Acetate [$Ba(CH_3COO)_2$], Strontium Acetate [$Sr(CH_3COO)_2$] and Titanium Iso-propoxide [$Ti(C_{22}O_4H_{28})$] powder are needed.

2.1.2. Weighing and mixing solution materials $Ba_{0.5}Sr_{0.5}TiO_3$ with RuO_2 6%.

The second stage is a weighing procedure (using an analytical balance) and mixing of the materials used. To produce a solubility of 1 M, the composition of the ingredients used, among others: Barium Acetate [$Ba(CH_3COO)_2$] 99% with a mass of 0.165 gr; Strontium Acetate [$Sr(CH_3COO)_2$] 99% with a mass of 0.5524 gr; Titanium Iso-propoxide [$Ti(C_{22}O_4H_{28})$]

99% with a mass of 0.3563 gr; 2-metoksietanol [$CH_3OCH_2CH_2OH$] 99% as much as 2.5 mL; Rubium Dioksida (RuO_2) with a mass of 0.0295 gr.

The mixing procedure was carried out based on the composition of the resulting BST solution (with 6% RuO_2 byproduct). RuO_2 doped of 6% is the best result of previous research [1]. The mixing procedure of this solution was stirred using a Branson model 2510 ultrasonicator for 60 minutes to obtain a homogeneous solution.

Previous research [1] concluded that 6% RuO_2 doping was the best doping among 2% RuO_2 doping, 4% RuO_2 doping, and no doping. In the article [1], the BST+RuO_2 variation film was characterized for its sensitivity as a light sensor. The results showed that the 6% BST+RuO_2 film had better sensitivity to changes in light intensity than other doping variations. The test is carried out using a forward-biased and reverse-biased circuit.

The test results with forwarding bias have a greater sensitivity value than the backward bias measurement. This is because when the forward bias condition (p-type Si is connected to V(+), n-type BST is connected to V(-)), current will flow from the cathode to the anode, so the film is a conductor. The explanation above concludes why only 6% RuO_2 doping concentration is used, as well as the reason why sensitivity testing is only carried out using a forward-biased circuit.

This research focuses more on variations in annealing temperature, namely 800°C, 850°C, and 900°C, for manufacturing BST + RuO_2 6%, which is then implemented as a light detection sensor.

2.1.3. Growth of $Ba_{0.5}Sr_{0.5}TiO_3$ thin film in 6% RuO_2.

The third stage is the process of growing a thin film layer for the annealing process. The process of growing a thin film layer consists of two steps, namely: Chemical Solution Deposition (CSD) of BST solution (with 6% RuO2 fork) on a 1×1 cm2 p-type Si(100) substrate (1/2 part of the substrate size); Screening (spin coating technique) p-type Si(100) substrate, which has been dripped with BST solution (with 6% RuO2 excision) using a spin coater with a speed of 3000 rpm for 30 seconds.

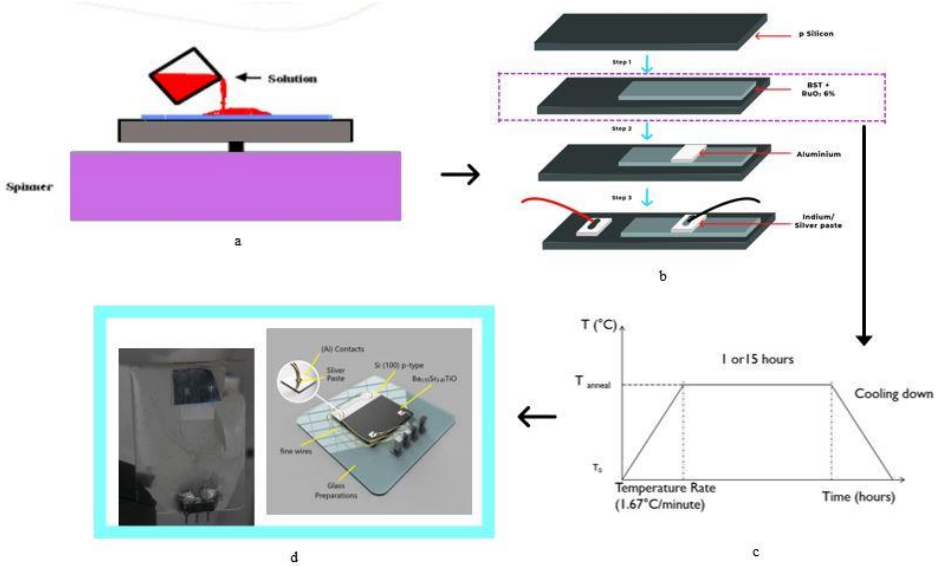

Figure 2. BST thin film fabrication methods with 6% RuO_2: **(a)** deposition/drop and rotating (spin coating technique); **(b)** results of deposition/drop and screening (spin coating technique); **(c)** annealing (temperature variation: 800°C, 850°C, and 900°C) and **(d)** thin film BST with 6% RuO_2.

The deposition/dropping and screening procedures were repeated three times with a pause of one minute. The thin film that has passed the Chemical Solution Deposition (CSD) process and spin coating technique is then annealed [28,29] using a furnace for 15 hours at temperatures of 800ºC, 850ºC, and 900ºC.

The description of the deposition/dropping method and screening (spin coating technique) to obtain a thin film is shown in Figure 2.

2.2. Mechanical design of BST + $RuO_2$6% film and solar tracker system using BST + 6% RuO_2 light sensor in ALSINTAN.

The design of the BST film and solar tracker system is divided into two parts, electronic circuit design and mechanical design of the tool system. Three components are needed to design electronic circuits: input, process, and output. More specifically, the solar tracker system's block diagram and the solar tracker system and the design of the solar tracker system using the RuO2 BST light sensor for ALSINTAN are shown in Figures 3 and 4.

Figure 3 explains the block diagram of the solar tracker system, that four BST + 6% RuO_2 sensors, which function as inputs, will read the intensity of sunlight continuously. Suppose one of the BST + RuO2 6% sensors reads a greater value than the other three BST + RuO2 6% sensors.

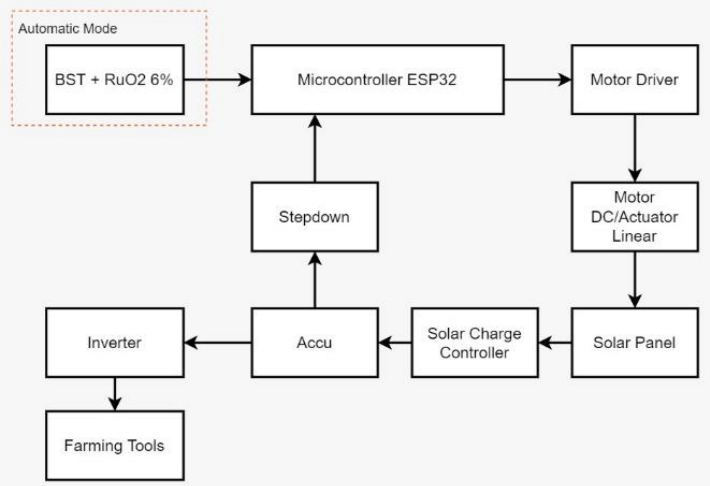

Figure 3. Block diagram of the solar tracker system.

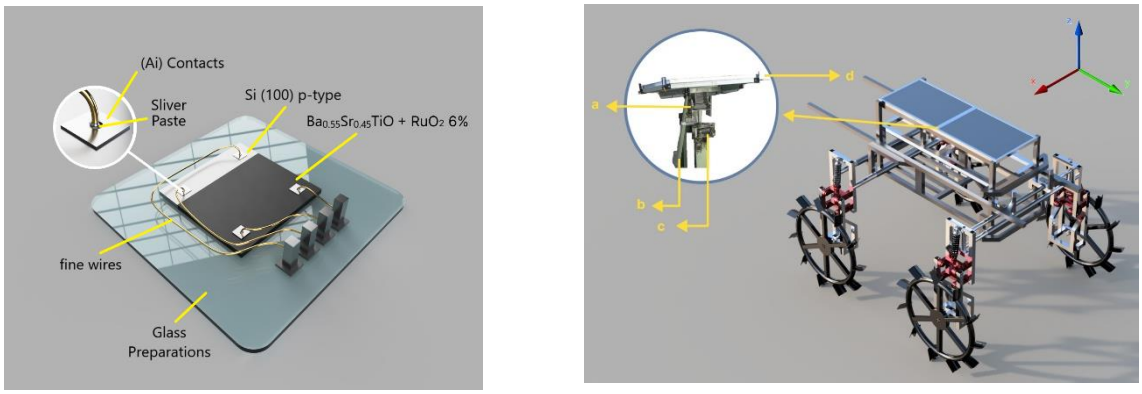

(a) (b)

Figure 4. Solar tracker system design using BST light sensor in RuO_2 for ALSINTAN: **(a)** BST + RuO_2 6%; **(b)** solar tracker system at ALSINTAN.

In that case, the microcontroller (as a processor) will analyze the sensor reading value data and instruct the output section, namely the dc motor/actuator, to move towards the direction of the highest 6% BST + RuO_2 value. The movement of the dc motor/actuator is in line with the movement of the solar panel towards the direction of the highest 6% BST + RuO_2 value. The output of electrical power generated by the solar panel is then used to charge the battery. This battery power will later be used for the electronic system for spraying pesticides on ALSINTAN.

Figure 4(a) explains that accu as a power supply comes from solar energy sources. Four BST + 6% RuO_2 sensors function as electronic components that will determine the movement of the motor toward the sunlight source. The logic of reading four BST + 6% RuO_2 sensors for motor movement is shown in Figure 3. The purpose of using BST + 6% RuO_2 sensors in this solar tracker system is to optimize the battery charging process and avoid damage to batteries that are often not charged due to bad weather conditions.

Figure 4(b) explains that the solar tracker determines the mechanical movement of the solar panels. The solar tracker moves using two actuators having a thrust of 1500N for driving on the x and y axes [38] with each movement angle of -15^o to +15^o. In Figure 4(b), part b shows the actuator that moves the solar panel to the y-axis by pushing the bracket (shown by part a). Part c shows the actuator that moves the solar panel to the x-axis. Section d shows the bracket for the BST + RuO_2 sensor.

2.3. Characterization of thin film BST with RuO_2 6% as a light detection sensor and testing of solar tracker systems using BST light sensors with 6% RuO_2 in ALSINTAN.

Thin film characterization of BST + RuO_2 6% was carried out to obtain the best sensor (a strong sensor when given continuous light intensity, a sensor with a constant hysteresis value, and a sensor with a response a 10-bit microcontroller can read). Characterization was carried out on each sample of 6% BST + RuO_2 sensor (annealing variations 800^{o}C, 850^{o}C, and 900^{o}C).

To get the best sensor in question, then there are three characterizations of electrical properties: Characterization of BST + RuO_2 6% thin film sensitivity as a light detection sensor; Hysteresis characterization (monotone up and monotone down); Strength characterization/life span of 6% BST + RuO_2 sensor (treatment for two weeks).

2.4. Testing the mechanical design model of the sensor case BST + RuO_2 6%.

This test is carried out to obtain the optimal value (output voltage value) from the light intensity reading by the BST + RuO_2 6% sensor, which is not influenced by other factors (temperature and pressure).

The sensor casing design model will certainly affect the sensor's performance while working, so it is necessary to test several casing design models. The casing design to be tested consists of an innovative casing design (Figure 8(a)), a closed casing design [39], and a casing design without a casing.

2.5. Testing the solar tracker system using BST light sensor with RuO_2 6% for ALSINTAN.

Testing the solar tracker system consists of: Electronic Circuit of Solar Tracker System using BST Light Sensor with RuO_2 6%; measurement of the value of the output voltage and current generated (without a solar tracker and using a solar tracker).

3. Results and Discussion

3.1. Characterization of electrical properties.

3.1.1. Thin film sensitivity BST + 6% RuO_2 as Light Detection Sensor.

Sensitivity is a comparison between the response of an instrument to changes in the variables that are input in the measurement. In other words, sensitivity is the ratio between the input and output signals. The sensitivity level is determined by the ratio between input and output [1,10,30]. This study's input signal is the light intensity (lumen). At the same time, the output signal is voltage (mV).

Sensitivity testing was carried out on BST, which was treated with 6% RuO_2. Thin film fabrication by extracting 6% RuO_2 material into BST solution is the best concentration value from the results of previous research [1]. In this study, the sensitivity level of the BST + RuO_2 sensor was 6% which was grown through annealing temperatures of 800°C, 850°C, and 900°C.

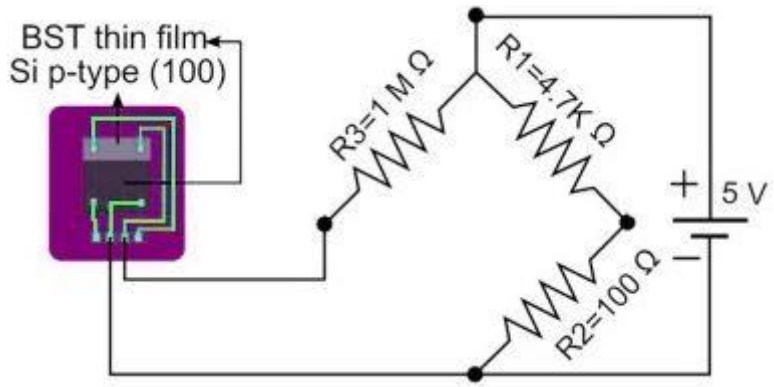

Figure 5. Forward bias circuit for thin film sensitivity testing BST + 6% RuO_2.

Testing the sensitivity of the BST + RuO_2 6% sensor is carried out using a forward bias circuit, as shown in Figure 5. Forward bias is a condition where the BST + RuO_2 6%) sensor as a photodiode can conduct electric current from the anode side (p-type Si) to the side. Cathode (BST + RuO_2 6%) without any resistance. Previous studies have shown that sensitivity testing using a forward bias circuit has a better sensitivity level than a reverse bias circuit [1, 39]. This is because if the BST thin film is given a positive voltage, the current will increase by itself. The current will increase rapidly if the voltage has reached its cut-in voltage value. This can happen because the voltage applied to a BST thin film has reached its cut-in value, so the barrier potential at the junction will react so that the BST current can flow quickly.

Figure 5 describes sensitivity testing assisted with the help of a Wheatstone bridge circuit. [1, 39] in his research explained that because BST has a resistance of around 106 ohms, the amount of resistance R1 can be found by the equation $R_1.R_{BST} = R_2.R_3$.The results of the sensitivity test for BST + RuO_2 thin film 6% with variations in annealing temperature (800°C, 850°C, and 900°C) are shown in Table 1. The test was carried out in two conditions, namely light (652 lumens) and dark conditions (2 lumens). The greater the voltage difference, the higher the film sensitivity is assumed to be. Table 1 shows that the sample treated with an annealing temperature of 850°C is the best film as a light detection sensor. This is because electrons excited to the conduction band will increase the charge carriers' electrical conductivity.

Table 1. Thin film sensitivity BST + RuO_2 6%.

Annealing Temperature (ºC)	Film to-		Output voltage (mv)	Voltage Difference (mv)	Intensity Difference (Lumen)	Sensitivity Level (mV/lumen)
800	1	Dark	0.10	0.01	650.00	1.54×10^{-5}
		Bright	0.11			
	2	Dark	0.10	0.00	650.00	0.00000
		Bright	0.10			
	3	Dark	0.15	0.02	650.00	3.08×10^{-5}
		Bright	0.17			
850	1	Dark	0.03	0.04	650.00	6.15×10^{-5}
		Bright	0.07			
	2	Dark	0.09	0.03	650.00	4.62×10^{-5}
		Bright	0.12			
	3	Dark	0.02	0.06	650.00	9.23×10^{-5}
		Bright	0.08			
900	1	Dark	0.17	0.02	650.00	3.08×10^{-5}
		Bright	0.19			
	2	Dark	0.15	0.01	650.00	1.54×10^{-5}
		Bright	0.16			
	3	Dark	0.17	0.03	650.00	4.62×10^{-5}
		Bright	0.20			

Researchers tested Scanning Electron Microscopy (SEM) to determine the microstructure of the 6% BST+RuO_2 film grains at each annealing temperature (800ºC, 850ºC, and 900ºC). Grain size varies from large to small. Tests were carried out at a magnification of 10000x. More specifically, the results of the SEM test are shown in Figure 6.

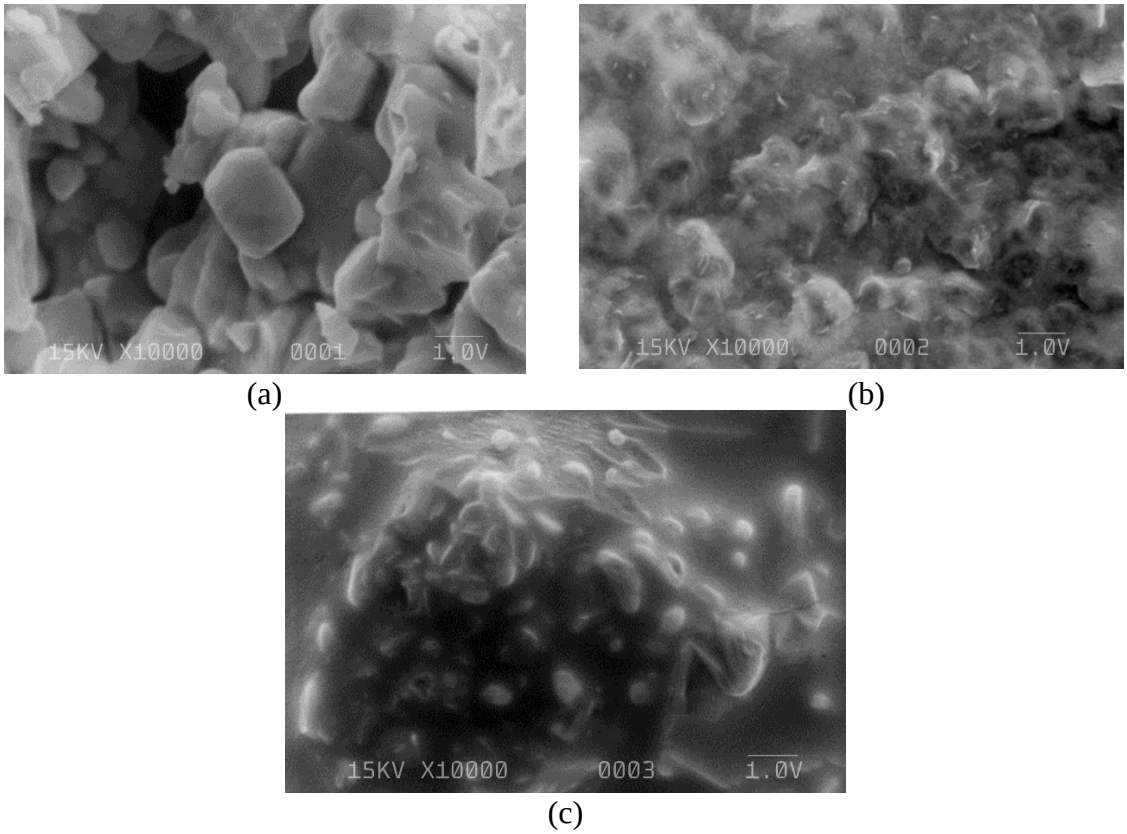

(a) (b)

(c)

Figure 6. SEM results of 6% BST+RuO_2 film: (**a**) Annealing temperature 800ºC; (**b**) Annealing temperature of 850ºC; and (**c**) Annealing temperature of 900ºC.

Figure 6 shows the SEM results of the annealing temperature variation of the surface microstructure of the 6% BST+RuO_2 film. At the annealing temperature of 850ºC, the grain size looked more uniform than at the annealing temperatures of 800ºC and 900ºC. The grain

size varies more at annealing temperatures of 800°C and 900°C. The increase in annealing temperature affects the shape of the grain size of the film structure; as shown in Figure 6, the grains become denser, regular, and homogeneous. However, an excessive increase in annealing temperature can degrade the microstructure of the film surface.

The increase in sensitivity can be attributed to the grains' density, regularity, and homogeneity. The more dense, regular, and homogeneous grain size can make the distance between grains closer so that the potential barrier between grains gets smaller. This causes the electron transfer process to be faster. So it was concluded that from the results of SEM testing on 6% BST+RuO_2 film, the best film was the one that was annealed at a temperature of 850°C, which the researchers called the optimum annealing temperature for this film.

3.1.2. Hysteresis sensor BST + RuO_2 6%.

Hysteresis testing was carried out to determine the accuracy of the 6% BST+RuO_2 sensor in varying stimulation readings (light intensity). Sensors with good hysteresis are sensors with a small difference in values when the measurement is monotonous up and monotone down.

Hysteresis testing is carried out until the maximum condition of the sensor can no longer respond to stimuli (light intensity). From this test, in addition to getting the voltage difference between monotonous up and monotone down, it is also obtained a wide range of readings of light intensity. The results of the hysteresis test for the BST + RuO_2 sensor 6% are shown in Figure 7.

In testing this hysteresis characteristic, the test results are said to be good if a similar sensor output voltage value is obtained when the sensor receives the same intensity, even though the intensity changes from low to high or vice versa. Thin films with an annealing temperature of 850°C showed a low hysteresis curve with a hysteresis index of 0.02%, while the annealing temperatures of 800°C and 900°C were 0.17% and 0.25%, respectively. We assume the low hysteresis comes from the thin-film paraelectric phase at room temperature. In this phase, the thin film is observed at temperatures above the curie temperature.

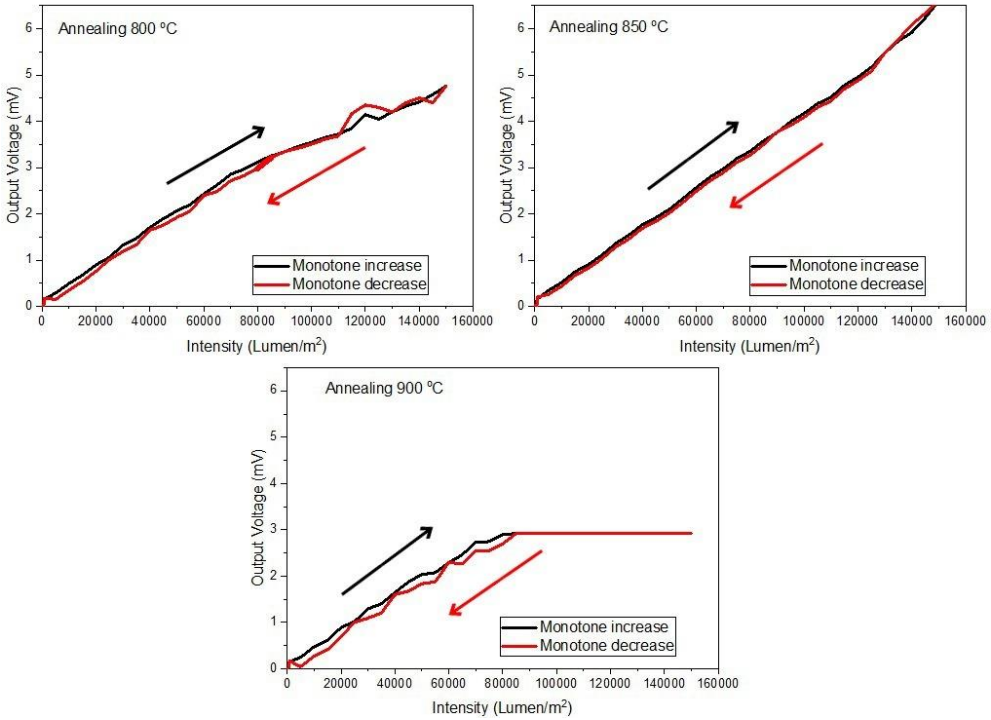

Figure 7. Results of hysteresis sensor BST + 6% RuO_2.

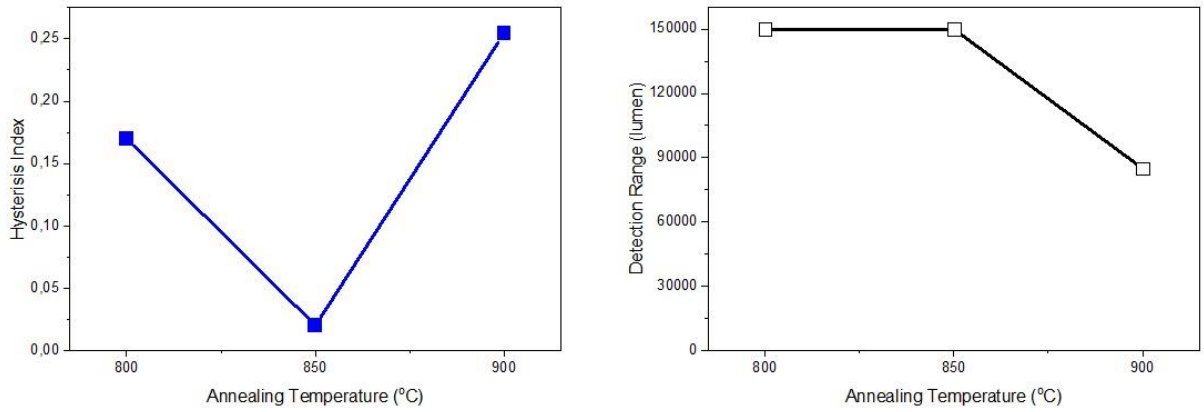

Figure 8. Hysteresis index and detection range of BST thin film with various annealing temperatures.

The range is determined based on the saturation condition of the output voltage, either when the light intensity increases or decreases. The lowest intensity that causes saturation is the maximum intensity the BST sensor can detect. That intensity is called the 6% BST + RuO2 thin film detection range. Figure 8 shows the detection range of each 6% BST + RuO_2 thin film. It was found that 6% BST + RuO_2 thin film with annealing temperatures of 800°C and 850°C had the highest detection range compared to 6% BST + RuO_2 thin film with annealing temperature of 900°C Although 6% BST + RuO_2 thin films with annealing temperatures of 800°C, and 850°C have the same detection range, 6% BST + RuO_2 films with annealing temperatures of 850°C have better hysteresis. Therefore, for all the advantages of BST + RuO_2 6% film with an annealing temperature of 850°C, this thin film is more appropriate to be used as a light detection sensor.

3.1.3. Power/Lifetime sensor BST + RuO_2 6%.

The strength/life span of the 6% BST + RuO_2 sensor with annealing temperatures of 800°C, 850°C, and 900°C was compared with the Light Dependent Resistor (LDR) sensor for two weeks. The strength/life span of the sensor is said to be good if the response value does not change from each stimulus (with the same light intensity value).

The results of the strength/life span of the 6% BST + RuO_2 sensor with annealing temperatures of 800°C, 850°C, and 900°C compared with the LDR sensor are shown in Figure 9. The test was carried out for two weeks, with the measurement time starting from 07.00 AM to 5.00 PM daily.

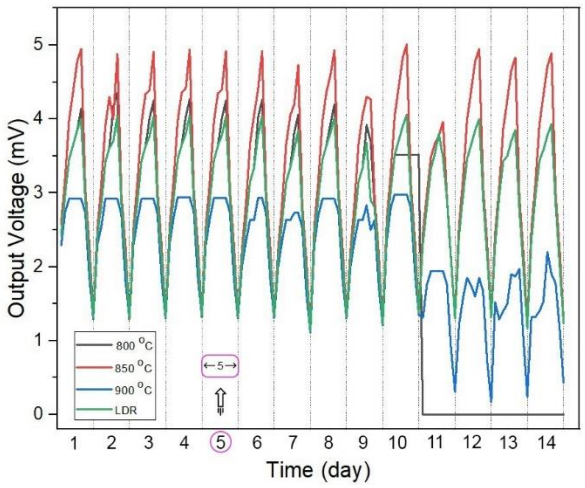

Figure 9. Strength test results/lifespan of thin film BST + 6% RuO_2 with annealing temperatures of 800°C, 850°C, and 900°C versus LDR sensor.

Figure 9 explains that BST + 6% RuO_2 thin film with an annealing temperature of 850°C and LDR sensor has a relatively more consistent output voltage value for two weeks of measurement. Thin film BST + RuO_2, 6% with annealing temperatures of 800°C and 900°C, simultaneously decreased performance on the 11th day. Even for thin film BST + RuO_2 6% with annealing temperature of 800°C drop to 0 mV output voltage value (damaged).

The graph of the strength/life span of the thin film BST + RuO_2, 6% with an annealing temperature of 850°C, is still better than the graph of the strength/life span of the LDR sensor. This is indicated by the sensitivity value of the sensor (width of the output voltage value) generated.

3.2. Testing the mechanical design model of the sensor case BST + RuO_2 6%.

Mechanical testing was carried out on the best film (BST + RuO_2 6% with an annealing temperature of 850°C). The optimization of the shape and design of the BST + RuO_2 sensor protection material 6% to be implemented on the solar tracker ALSINTAN pesticide sprayer needs to be studied to get the accuracy of the results of measuring the intensity of sunlight which is carried out continuously because BST gets two stimuli: light and temperature). The model and design material for the innovation casing is shown in Figure 10. Meanwhile, the results of the BST sensor measurement (variation of the casing model) with the treatment of sunlight intensity at certain hours are shown in Table 2.

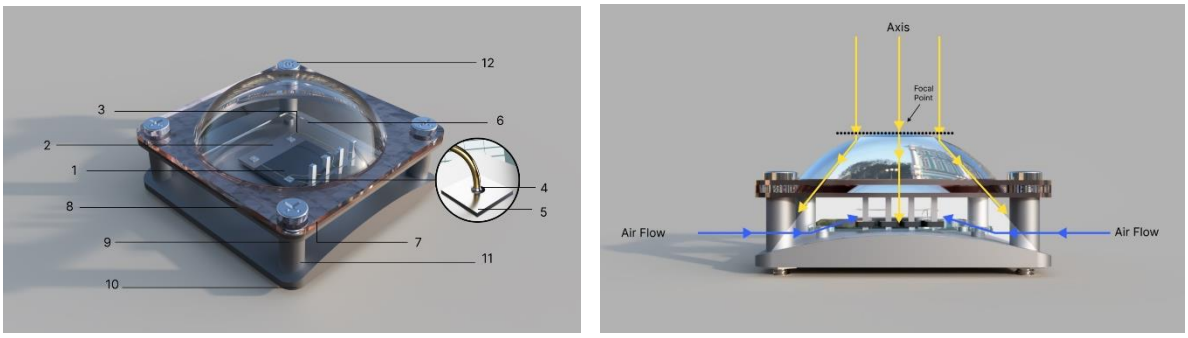

(a) (b)

Figure 10. Innovation case design models and materials: (**a**) casing parts; (**b**) illustration of light and heat working in design.

Table 2. Measurement results of the BST sensor (casing variation) with the treatment of sunlight intensity at certain hours.

Hour	*Innovation Case*			*Closed case**			*Without case*		
	Output voltage (mV)			Output voltage (mV)			Output voltage (mV)		
	Day to-1	Day to-2	Day to-3	Day to-1	Day to-2	Day to-3	Day to-1	Day to-2	Day to-3
08.00	2,57	2,49	2,53	2,57	2,46	2,52	2,49	2,47	-
09.00	3,19	3,18	3,21	3,19	3,08	3,17	3,16	3,17	-
10.00	3,99	2,85**	3,9	4,17	3,40**	4,09	3,96	-**	-
11.00	4,38	4,30	4,34	4,3	4,34	4,51	4,35	-	-
12.00	4,78	4,86	4,70	4,78	4,69	4,72	4,40	-	-
13.00	4,95	4,94	4,91	4,95	4,87	4,84	4,92	-	-
14.00	3,08	2,98	3,03	4,80	4,82	4,75	3,04	-	-
15.00	2,31	2,27	2,29	4,75	4,77	4,61	2,30	-	-
16.00	1,34	1,29	1,32	4,02	4,14	4,04	1,32	-	-

* casing model as done by [39].

** rainy weather conditions.

Figure 10(a) describes the parts that exist in the casing design model of the invention, namely: (1) is BST + RuO_2 6% with annealing of 850°C, (2) is Si (100) p-type, (3) is fine wires,

(4) is a silver paste, (5) is Ai contact, (6) is glass preparation, (7) is a concave-convex lens, (8) is upper conductor, (9) is a lower conductor, (10) is the bottom case, (11) is the aluminum spacer, and (12) is the bolt.

This innovation casing model was tested to obtain the sensitivity and accuracy of the data from the BST + RuO_2 sensor reading 6% with an annealing temperature of 850^oC to the response of the intensity of sunlight without any other response disturbances (temperature and pressure). The choice of concave-convex lens model is used because it has the property of spreading light. The working principle of this innovative casing design model is more clearly shown in Figure 10(b).

The results of testing the innovation casing design model and without casing show that the output voltage value has a similar pattern; namely, the voltage increases when the intensity of sunlight increases and vice versa. The results of reading BST + RuO_2 6% on "without casing" on the 2nd and 3rd days did not produce an output voltage value because the BST condition was damaged after being exposed to rainwater.

In contrast to the test results on the closed casing design model, the output voltage value generated each time treatment is quite strange. The intensity of sunlight at 8.00 and 16.00 of 51900 lumens and 57000 lumens produces much different output voltage values. This shows that the temperature response influences reading. So it is concluded that the innovative casing design model is suitable to be implemented on the ALSINTAN pesticide spraying solar tracker.

3.3. Solar tracker system testing using BST + 6% RuO_2 light sensor for ALSINTAN.

3.3.1. Electronic circuit of solar tracker system using BST + 6% RuO_2 light sensor.

The solar tracker's electronic circuit requires several components, as shown in Figure 11. Each electronic component is integrated with the ESP32 because of the ESP32 (type of microcontroller used). The BST + RuO_2, 6% sensor, is connected to ESP32 as input, while the motor driver, DC motor, and actuator are connected as output. In principle, solar panels mounted with 6% BST + RuO_2 sensors at each corner will read the value of the intensity of sunlight. The intensity value will be processed and processed by the microcontroller.

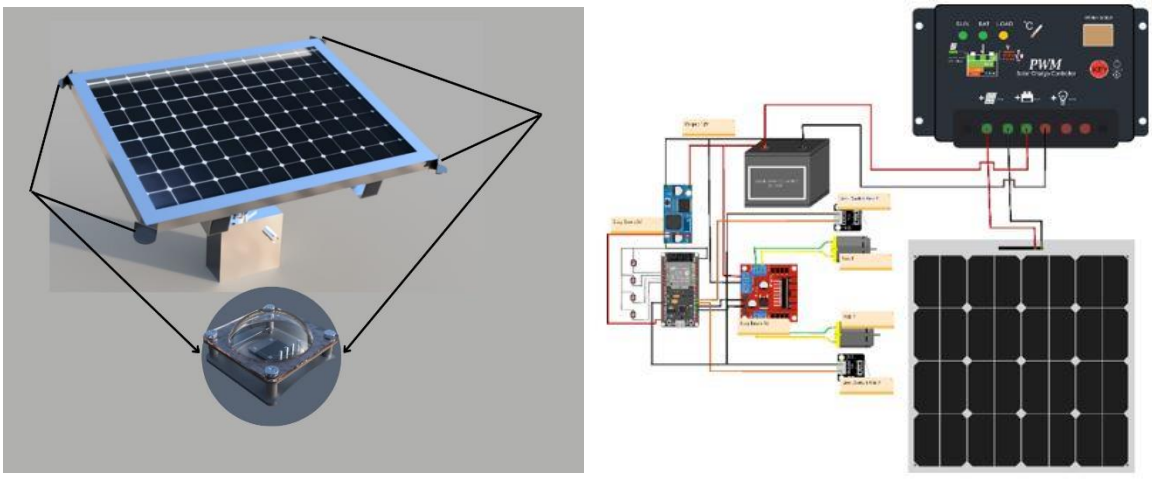

(a) (b)

Figure 11. **(a)** Design Model of 6% BST + RuO_2 Sensor Placement on Solar Tracker; (**b**) Electronic Circuit of Solar Tracker System for ALSINTAN Pesticide Sprayer.

The microcontroller will compare the input intensity values from each sensor. The largest value among the four sensors is the command for the actuator to move the surface position of the solar panel to face the greatest light intensity. Thus, the current and voltage generated by the solar panel will have maximum performance compared to solar panels that are only silent (static). A more detailed illustration of the BST + RuO_2 6% solar tractor sensor design model and an electronic circuit is shown in Figure 11.

3.3.2. Measurement of output voltage and current value (without solar tracker and using solar tracker).

This test is carried out to obtain the voltage and current value on the solar panel output probe, either without a solar tracker or with a solar tracker. The measurement data was carried out nine times (8:00 AM; 09.00 AM; 10.00 AM; 11.00 AM; 12.00 AM; 01.00 PM; 02.00 PM; 03.00 PM, and 04.00 PM). The type of solar panel used is Poly solar panel 50Wp Kawachi brand. Figure 12 (graph of time vs. output voltage) shows the trend of decreasing the value of the voltage, which is much gentler in the system using a solar tracker (shown at 01.00 PM and 02.00 PM). Even the output voltage results carried out nine times on a system that uses a solar tracker are always higher than those without a solar tracker. This shows that the BST + RuO_2 film implemented in the solar tracker system functions well as a light detection sensor. Even though the graph of the electric current produced has a similar curve shape, the value of the electric current generated is greater when using a solar tracker system.

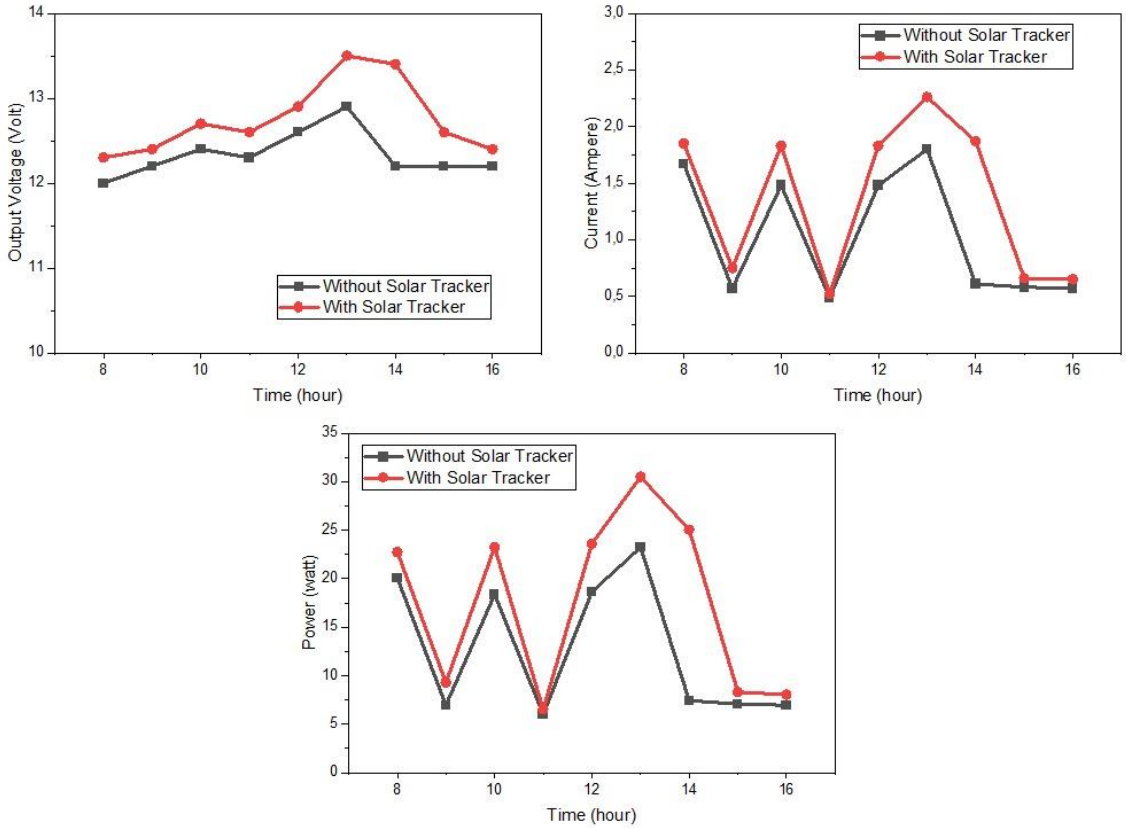

Figure 12. Solar panel measurement results: voltage value, current value, and power value.

Thus, based on the output voltage and current data generated from nine measurements, the implementation of the solar tracker system is much better than without a solar tracker. Besides being seen in Figure 12 (time vs. power graph), this is also proven through power

optimization calculations. The results of the power optimization calculation found that the use of a solar tracker and those without a solar tracker had a power difference of 37.21%.

4. Conclusions

The ferroelectric sensor made of BST + RuO_2 thin film 6% with an annealing temperature of 850^{o}C has excellent characterization to be applied as a light detection sensor in solar trackers for ALSINTAN. This thin film has the highest sensitivity, lowest hysteresis, highest detection range, and long strength/life span compared to other thin films. This 6% BST + RuO_2 thin film with an annealing temperature of 850^{o}C has been successfully applied as a light detection sensor on a solar tracker for ALSINTAN. The results of the power optimization calculation found that the use of a solar tracker and those without a solar tracker had a power difference of 37.21%.

Funding

This research was funded by Hibah Program Kompetitif Nasional Skema Penelitian Disertasi Doktor (PDD), grant number 0267/E5/AK.04/2022, dated April 28, 2022, Kementerian Pendidikan, Kebudayaan, Riset, dan Teknologi Republik Indonesia.

Acknowledgments

We gratefully acknowledge the funding from Hibah Program Kompetitif Nasional Skema Penelitian Disertasi Doktor (PDD) with grant number 0267/E5/AK.04/2022, dated April 28, 2022, Kementerian Pendidikan, Kebudayaan, Riset, dan Teknologi Republik Indonesia.

Conflicts of Interest

The authors declare no conflict of interest

References

1. Siskandar, R.; Dio, F.C.; Alatas, H.; Irzaman Application of Ba0.5Sr0.5TiO3 (BST) Film Doped With RuO2 (0%, 2%, 4% and 6%) On A Rice-Stalk Cutting Robot Model Based On A Line Follower With Hc-05 Bluetooth Control. *BIOINTERFACE Res. Appl. Chem.* **2022**, *12*, 2138–2151.
2. Szafraniak, B.; Fusnik, L.; Xu, J.; Gao, F.; Brudnik, A.; Rydosz, A. Semiconducting Metal Oxides: SrTiO3, BaTiO3 and BaSrTiO3 in Gas-Sensing Applications: A Review. *Coating* **2021**, *11*, 1–22.
3. Naghizade, S.; Sattari-Esfahlan, S.M. An Optical Five Channel Demultiplexer-Based Simple Photonic Crystal Ring Resonator for WDM Applications. *J. Opt. Commun.* **2020**, *41*, 37–43, https://doi.org/10.1515/joc-2017-0129.
4. Liu, Y.R.; Ren, L.F.; Yang, R.H.; Han, J.; Yao, R.H.; Wen, Z.C.; Xu, H.H.; Xu, J.X. Effects of Annealing Temperature on Electrical Properties of ZnO Thin-Film Transistors. *nanomaterials* **2022**, *12*, 1–11, https://doi.org/10.3969/j.issn.1000-565X.2011.09.018.
5. Karthikeyan, S.; Hwang, S.; Sibakoti, M.; Bontrager, T.; Liptak, R.W.; Campbell, S.A. Effect of Rapid Thermal Annealing of Copper Indium Aluminium Gallium Diselenide Solar Cell Devices and Its Deposition Challenges. *Appl. Surf. Sci.* **2019**, *493*, 105–111, https://doi.org/10.1016/j.apsusc.2019.06.279.
6. Afify, H.H.; Hassan, M.E.; M.badr, A.; Elsheikh, H.A. Effect of Hydrogen on Pristine Amorphous v 2 O 5 Thin Film. *Materials (Basel).* **2022**, *7*, 1–5, https://doi.org/10.18576/ijtfst/070101.
7. Asbani, B.; Robert, K.; Roussel, P.; Brousse, T.; Lethien, C. Asymmetric Micro-Supercapacitors Based on Electrodeposited Ruo2 and Sputtered VN Films. *Energy Storage Mater.* **2021**, *37*, 207–214, https://doi.org/10.1016/j.ensm.2021.02.006.
8. Asbani, B.; Buvat, G.; Freixas, J.; Huvé, M.; Troadec, D.; Roussel, P.; Brousse, T.; Lethien, C. Ultra-High Areal Capacitance and High Rate Capability RuO2 Thin Film Electrodes for 3D Micro-Supercapacitors. *Energy Storage Mater.* **2021**, *42*, 259–267, https://doi.org/10.1016/j.ensm.2021.07.038.
9. Kutsuzawa, D.; Oka, D.; Fukumura, T. Thickness Effects on Crystal Growth and Metal–Insulator Transition in Rutile-Type RuO2 (100) Thin Films. *Phys. Status Solidi Basic Res.* **2020**, *257*, 1–5,

https://doi.org/10.1002/pssb.202000188.
10. Ismangil, A.; Prakoso, W.G. The Effect of Electrical Conductivity of LiTaO 3 Thin Film to Temperature Variations. **2020**, *29*, 3234–3240.
11. Falmbigl, M.; Golovina, I.S.; Plokhikh, A. V.; Imbrenda, D.; Podpirka, A.; Hawley, C.J.; Xiao, G.; Gutierrez-Perez, A.; Karateev, I.A.; Vasiliev, A.L.; et al. BaTiO3 Thin Films from Atomic Layer Deposition: A Superlattice Approach. *J. Phys. Chem. C* **2017**, *121*, 16911–16920, https://doi.org/10.1021/acs.jpcc.7b05633.
12. Konsago, S.W.; Žiberna, K.; Kmet, B.; Benčan, A.; Uršič, H.; Malič, B. Chemical Solution Deposition of Barium Titanate Thin Films with Ethylene Glycol as Solvent for Barium Acetate. *Molecules* **2022**, *27*, 3753, https://doi.org/10.3390/molecules27123753.
13. Tang, X.; Li, K.H.; Liao, C.H.; Taboada Vasquez, J.M.; Wang, C.; Xiao, N.; Li, X. Chemical Solution Deposition of Epitaxial Indium- and Aluminum-Doped Ga2O3 Thin Films on Sapphire with Tunable Bandgaps. *J. Eur. Ceram. Soc.* **2022**, *42*, 175–180, https://doi.org/10.1016/j.jeurceramsoc.2021.09.064.
14. Bruneel, E.; Rijckaert, H.; Sierra, J.D.; Buysser, K. De; Driessche, I. Van An Evaluation of Nanoparticle Distribution in Solution-Derived YBa2Cu3O7−δ Nanocomposite Thin Films by XPS Depth Profiling in Combination with TEM Analysis. *crystals* **2022**, *12*, 80–83, https://doi.org/10.7868/s0207352816040211.
15. Julien, C.M.; Mauger, A.; Hussain, O.M. Sputtered LiCoO2 Cathode Materials for All-Solid-State Thin-Film Lithium Microbatteries. *Materials (Basel).* **2019**, *12*, 1–26, https://doi.org/10.3390/ma12172687.
16. Gudkov, S.I.; Solnyshkin, A. V.; Kiselev, D.A.; Belov, A.N. Electrical Conductivity of Lithium Tantalate Thin Film. *Ceramica* **2020**, *66*, 291–296, https://doi.org/10.1590/0366-69132020663792885.
17. Dey, S.K.; Kooriyattil, S.; Pavunny, S.P.; Katiyar, R.S. Analyses of Substrate-Dependent Broadband Microwave (1–40 GHz) Dielectric Properties of Pulsed Laser Deposited Ba0.5Sr0.5TiO3 Films. *crystals* **2021**, *15*, 1–23.
18. Panomsuwan, G.; Manuspiya, H. Morphological and Structural Properties of Barium Strontium Titanate Nanopowders Synthesized via a Sol-Gel Method. *Ferroelectrics* **2020**, *554*, 30–37, https://doi.org/10.1080/00150193.2019.1684763.
19. Hamdani, A.; Komaro, M.; Irzaman A Synthesis of BaXSr1-XTiO3 Film and Characterization of Ferroelectric Properties and Its Extension as Random Access Memory. *Mater. Phys. Mech.* **2019**, *42*, 131–140, https://doi.org/10.18720/MPM.4212019_11.
20. Anindy, U.; Nur Indro, M.; Husein, I. Piezoelectric Properties: Cerium Oxide (CeO2) Doped Barium Titanate (BaTiO3) Film on ITO Substrate. *Ferroelectrics* **2021**, *570*, 162–175, https://doi.org/10.1080/00150193.2020.1839267.
21. Kheyrdan, A.; Abdizadeh, H.; Shakeri, A.; Golobostanfard, M.R. Structural, Electrical, and Optical Properties of Sol-Gel-Derived Zirconium-Doped Barium Titanate Thin Films on Transparent Conductive Substrates. *J. Sol-Gel Sci. Technol.* **2018**, *86*, 141–150, https://doi.org/10.1007/s10971-018-4610-5.
22. Thakre, A.; Kumar, A. Enhanced Bipolar Resistive Switching Behavior in Polar Cr-Doped Barium Titanate Thin Films without Electro-Forming Process. *AIP Adv.* **2017**, *7*, https://doi.org/10.1063/1.5004232.
23. Arunkumar, D.R.; Anjelin Ursula Portia, S.; Ramamoorthy, K. Design and Fabrication of Novel Tb Doped BaTiO3 Thin Film with Superior Light-Harvesting Characteristics for Dye Sensitized Solar Cells. *Surfaces and Interfaces* **2021**, *22*, 100853, https://doi.org/10.1016/j.surfin.2020.100853.
24. Korobova, N.; Timoshenkov, S.; Artemov, E.; Kosolapova, G.; Petrova, V. Preparation and Some Properties of Pure and Doped Barium Titanate Thin Films. *2015 IEEE 35th Int. Conf. Electron. Nanotechnology, ELNANO 2015 - Conf. Proc.* **2015**, 204–206, https://doi.org/10.1109/ELNANO.2015.7146872.
25. Sharma, S.; Tomar, M.; Puri, N.K.; Gupta, V. Ultraviolet Radiation Detection by Barium Titanate Thin Films Grown by Sol-Gel Hydrothermal Method. *Sensors Actuators, A Phys.* **2015**, *230*, 175–181, https://doi.org/10.1016/j.sna.2015.04.019.
26. Bai, X.; Xu, M.; Li, Q.; Yu, L. Trajectory-Battery Integrated Design and Its Application to Orbital Maneuvers with Electric Pump-Fed Engines. *Adv. Sp. Res.* **2022**, *70*, 825–841, https://doi.org/10.1016/j.asr.2022.05.014.
27. Zhu, Y.; Liu, C.; Sun, K.; Shi, D.; Wang, Z. Optimization of Battery Energy Storage to Improve Power System Oscillation Damping. *IEEE Trans. Sustain. Energy* **2019**, *10*, 1015–1024, https://doi.org/10.1109/TSTE.2018.2858262.
28. Kurniawan, A.; Irzaman; Yuliarto, B.; Fahmi, M.Z.; Ferdiansjah Application of Barium Strontium Titanate (BST) as a Light Sensor on Led Lights. *Ferroelectrics* **2020**, *554*, 160–171, https://doi.org/10.1080/00150193.2019.1684758.
29. Setiawan, A.A.; Novitri; Irzaman; Zuhri, M.; Irmansyah; Alatas, H. Crystalline Structures Properties Doped RuO2 (0, 2, 4, 6%) of Thin Film LiNbO3. *J. Phys. Conf. Ser.* **2019**, *1282*, 6–12, https://doi.org/10.1088/1742-6596/1282/1/012059.
30. Ismangil, A.; Noor, F.A.; Winata, T. The Effect of Niobium and Rubidium Doping on the Energy Band Gap of a Lithium Tantalate (LiTaO3) Thin Film. *Indones. J. Phys.* **2021**, *32*, 1–5, https://doi.org/10.5614/itb.ijp.2021.32.2.1.